A micro-Raman study of a $Pr_{0.5}Ca_{0.5}MnO_3$ single crystal and thin films

2009 J. Phys.: Condens. Matter 21 386004

(http://iopscience.iop.org/0953-8984/21/38/386004)

J. Phys.: Condens. Matter **21** (2009) 386004 (6pp) doi:10.1088/0953-8984/21/38/386004

A micro-Raman study of a $Pr_{0.5}Ca_{0.5}MnO_3$ single crystal and thin films

S Mansouri[1], S Charpentier[1], S Jandl[1], P Fournier[1], A A Mukhin[2], V Yu Ivanov[2] and A Balbashov[3]

[1] Département de Physique, Université de Sherbrooke, 2500 Boulevard Université, Sherbrooke, Québec J1K 2R1, Canada
[2] General Physics Institute of the Russian Academy of Sciences, 38 Vavilov Street, 119991 Moscow, Russian Federation
[3] Moscow Power Engineering Institute, 14 Krasnokazarmennaya Street, 105835 Moscow, Russia

Received 25 May 2009
Published 27 August 2009
Online at stacks.iop.org/JPhysCM/21/386004

Abstract

We present a micro-Raman study of a high quality $Pr_{0.5}Ca_{0.5}MnO_3$ single crystal and thin films on $SrTiO_3$ and $LaAlO_3$ substrates. Ten A_g and seven B_{2g} Raman-active modes (simplified symmetry: $Pmma$ space group) have been observed and correlated to charge ordering around $T_{co} = 240$ K and antiferromagnetic spin–orbital ordering at $T_N \sim 170$ K. Our data reveal that coherent Jahn–Teller MnO_6 distortions prevail at $T < T_N$. Moreover, the temperature dependence of the frequency and linewidth of the A_g mode corresponding to in-plane oxygen atom rotation ($\sim$268 cm^{-1}) is analyzed within a polaron-like scheme that reflects a strong charge ordering to lattice coupling. The close similarities between the single crystal and the thin films' phonon evolution confirm that the thin films growth conditions have been optimized.

1. Introduction

Doped manganites $R_{1-x}A_xMnO_3$ (R = lanthanides and A = Ba, Sr or Ca) have been extensively investigated in the last decade because of their exciting properties such as colossal magnetoresistance, spin, orbital and charge orders [1–4]. Substitution of R^{3+} by A^{2+} generates Mn^{4+} ions leading to physical properties governed by competing effects from Jahn–Teller distortions, double exchange mechanism, ferromagnetism and metallicity due to substantial electron transfer from Mn^{3+} to Mn^{4+} [5, 6]. Temperature, doping and structural distortions quantified by the tolerance factor drive the doped manganites into a rich set of phases including a paramagnetic insulator, a ferromagnetic metal and a charge ordered antiferromagnetic insulator [7]. The colossal negative magnetoresistance that reflects strong coupling between the electrical and magnetic properties is observed near either the concomitant paramagnetic insulator–ferromagnetic metallic phase transition [8] or the ferromagnetic metallic–charge ordered insulator transition [9]. As a function of temperature and doping, the Mn^{3+}/Mn^{4+} distribution modifies the Mn–O–Mn bond length and angle and provokes a structural disorder. Hopping of an electron from an occupied Mn^{3+} e_g orbital to an adjacent Mn^{4+} unoccupied e_g orbital depends strongly on the MnO_6 octahedra relative tilting and the dynamic Jahn–Teller distortion that accompanies the moving electrons.

In particular, in $R_{0.5}Ca_{0.5}MnO_3$ half-doped manganites, ordering of the Mn^{3+} and Mn^{4+} ions as well as the Mn^{3+}d orbitals at low temperatures transforms the compounds into an insulating and CE-type antiferromagnet with static Jahn–Teller distortions [10]. Typically, at temperatures below 170 K a superstructure (space group $P2_1/m$) with doubled a lattice parameter of $RMnO_3$ ($Pnma$ unit cell) is formed [11, 12]. The charge order develops in the ac planes where each Jahn–Teller distorted $Mn^{3+}O_6$ octahedron is surrounded by four undistorted $Mn^{4+}O_6$ octahedra and vice versa. Rows of one type of octahedra are aligned along the b axis.

The $Pr_xCa_{1-x}MnO_3$ system exhibits colossal magnetoresistance for both electron and hole doping. It is characterized by equal Pr^{3+} and Ca^{2+} ionic radii (1.18 Å) with charge ordering occurring for $0.3 \leqslant x \leqslant 0.75$ in the 220–250 K temperature range. Within the charge order phase, a transition to an antiferromagnetic insulating phase occurs at $T_N < T_{co}$ and a strong magnetic field is needed to induce the transition to a metallic phase. In the intermediate range $T_N < T < T_{co}$,

orbital ordering sets in gradually until it is achieved around T_N. Also, the x-dependent metal–insulator phase diagram in the H–T plane indicates that a deviation of x from 0.5, where the carrier concentration is exactly commensurate with the number of ionic sites leading to Mn^{3+}/Mn^{4+} ordering, alters the robustness of the charge ordering state [13].

Recently, $Pr_{0.6}Ca_{0.4}MnO_3$ resonant x-ray diffraction [14], ^{17}O NMR study [15] and best fit of high resolution 10 K x-ray and neutron powder diffraction data of $Pr_{0.5}Ca_{0.5}MnO_3$ [16] have supported CE-type symmetry and the corresponding striped charge and orbital picture. Nevertheless, refined crystal structure of $Pr_{0.60}Ca_{0.40}MnO_3$ from neutron diffraction data [17] and $Pr_{1-x}Ca_xMnO_3$ ($0.3 \leqslant x \leqslant 0.5$) high resolution transmission electron microscopy [18] have suggested the trapping of electrons within pairs of Mn sites, involving both a local double exchange and a polaronic-like distortion (Zener polaron). Also, over wide doping and temperature ranges, phase coexistence between charge–orbital ordered $P2_1/m$ monoclinic and disordered $Pnma$ orthorhombic have been observed [18].

Strain effects on $Pr_{0.5}Ca_{0.5}MnO_3$ thin films have been recently studied [19, 20]. Grown on $LaAlO_3$ (LAO) substrates, these films presented a monoclinic distortion at room temperature as well as an unusual insulating ferromagnetic phase [19]. Using $SrTiO_3$ (STO) substrates, $Pr_{0.5}Ca_{0.5}MnO_3$ thin films are under tensile stress leading to a spectacular decrease of the charge ordered state melting magnetic field that controls the magnetoresistance, typically from 20 T in the bulk material down to 7 T in the films [20].

Raman spectroscopy has proved its efficiency in the characterization and study of various $RMnO_3$ and $R_{1-x}A_xMnO_3$ phases [21, 22]. Abrashev *et al* [23] have observed in $La_{0.5}Ca_{0.5}MnO_3$ that the new activated Raman modes, below $T \sim 150$ K, in the antiferromagnetic insulating ordered state were enhanced when excited with laser energies close to the Jahn–Teller gap of roughly 1.9 eV. Asselin *et al* [24] and Jandl *et al* [25] have shown that the $Nd_{0.5}Sr_{0.5}MnO_3$ and $Nd_{0.5}Ca_{0.5}MnO_3$ Raman-active phonons retrace the magnetic and structural temperature evolution in the paramagnetic, charge ordered and antiferromagnetic orbital ordering regimes. It must be emphasized here that, in addition to the $La_{0.5}Ca_{0.5}MnO_3$, $Nd_{0.5}Sr_{0.5}MnO_3$ and $Nd_{0.5}Ca_{0.5}MnO_3$ identical crystalline structures, phonon symmetries and MnO_6 octahedra stretching, bending and tilting frequencies in the CE-type phase indicate coherent cooperative Jahn–Teller distortions as well as strong similarities in Ca-and Sr-doped manganites charge and orbital orders. Also, the persistence at $T < T_N$ of phonons related to the high temperature ferromagnetic and A-type antiferromagnetic phases corroborates a scenario involving phase separation [26].

Dediu *et al* [27] have studied $Pr_{0.65}Ca_{0.35}MnO_3$ single-phase polycrystalline samples by Raman scattering as a function of temperature and excitation energy. The spectral shape and intensities were affected by the charge ordering and antiferromagnetic transitions, indicating strong charge–lattice and spin–lattice couplings. Gupta *et al* [28] have reported the evolution of Raman-active A_g phonon modes in $Pr_{0.63}Ca_{0.37}MnO_3$ as a function of temperature, revealing that their frequencies and unexpectedly linewidths increase as temperature decreases due to strong spin–phonon coupling. In contrast, Dattagupta and Sood [29] computed frequency shifts and linewidths focusing on charge fluctuations and concomitant charge ordering influenced by phonons in $Pr_{0.63}Ca_{0.37}MnO_3$.

Raman studies of charge and orbital ordering in manganite thin films are somehow contradictory with respect to single-crystal measurements. Raman spectra of $Nd_{0.5}Ca_{0.5}MnO_3$ thin films [30] are very similar to those of the single crystal [25] in retracing charge ordering and antiferromagnetic phase transitions, while the phonons in $La_{0.5}Ca_{0.5}MnO_3$ thin films [31] do not match those observed in the bulk [23]. Similarly, $Pr_{0.5}Ca_{0.5}MnO_3$ thin films grown on STO and LAO substrates show, between $T = 300$ K and 80 K, no significant spectra changes except in phonon intensities [32] and additional broad bands around 545, 615 and 680 cm^{-1} [33], in contrast to $Pr_{0.65}Ca_{0.35}MnO_3$ single-crystal Raman spectra [27].

In this paper we present a micro-Raman study of $Pr_{0.5}Ca_{0.5}MnO_3$ single crystal and thin films in order to retrace the impact of the charge ordered and antiferromagnetic phases as a function of temperature. The objectives are: (i) to detect, in comparison with $Nd_{0.5}Ca_{0.5}MnO_3$, the possible coexistence of charge–orbital ordered $P2_1/m$ monoclinic and disordered $Pnma$ orthorhombic structures that has been reported following controversial structural refinements in $Pr_{1-x}Ca_xMnO_3$ [18], (ii) to study the influence of charge ordering on phonon frequencies and linewidths by fitting them with available models and (iii) to compare our thin film response concerning the phase transitions with previous thin film studies [32, 33].

2. Experiment

The floating zone method was used to grow high quality $Pr_{0.5}Ca_{0.5}MnO_3$ single crystals [34]. $Pr_{0.5}Ca_{0.5}MnO_3$ (PCMO) 200 and 2000 Å thin films were grown by pulsed laser ablation deposition on $LaAlO_3$ (LAO) and $SrTiO_3$ (STO) [100] substrates using a KrF excimer pulsed laser at 10 Hz in 400 mTorr molecular oxygen pressure. All the films were grown at 820 °C for 2 and 20 min with an estimated growth rate of 1.7 Å s^{-1}, resulting in thicknesses of ∼200 and 2000 Å, respectively. We must emphasize that our thin film growth temperature is similar to that used previously in our work on $Nd_{0.5}Ca_{0.5}MnO_3$ [30] and is also higher than previous conditions used for $Pr_{0.5}Ca_{0.5}MnO_3$ in [32, 33]. The growth was followed by *in situ* fast cooling (∼40 °C min^{-1}) in 400 Torr of O_2 and a post-annealing step for 15–20 min at 400 °C. The films were then checked by x-ray diffraction to confirm their orientation and their actual lattice parameters.

Raman spectra with 0.5 cm^{-1} resolution were measured in the backscattering configuration using an He–Ne laser (632.8 nm) and a Labram-800 Raman microscope spectrometer equipped with a 50× objective, appropriate notch filter and nitrogen-cooled CCD detector. The laser power was kept at 0.8 mW to avoid local heating. The single crystals and thin films were mounted on the cold finger of a micro-helium Janis cryostat and A_g (xx) and B_{2g} (zx) symmetry

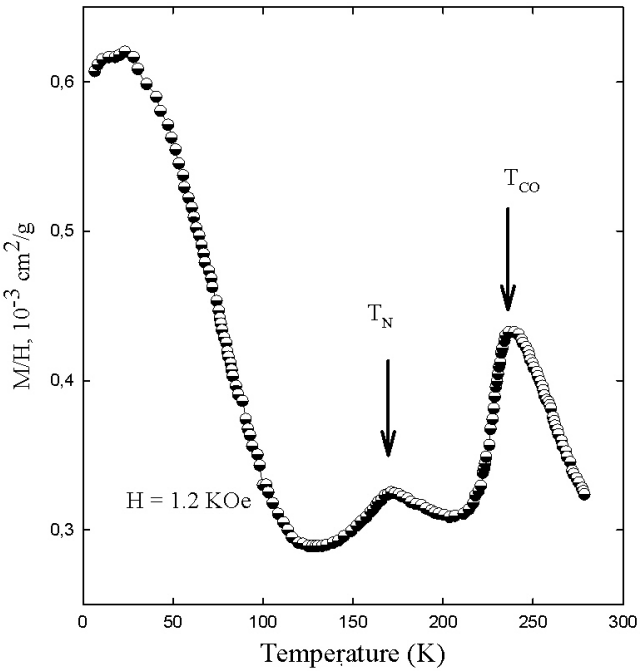

Figure 1. $Pr_{0.5}Ca_{0.5}MnO_3$ single-crystal DC susceptibility as a function of temperature. The phase transitions due to charge ordering (T_{co}) and antiferromagnetic ordering (T_N) are indicated.

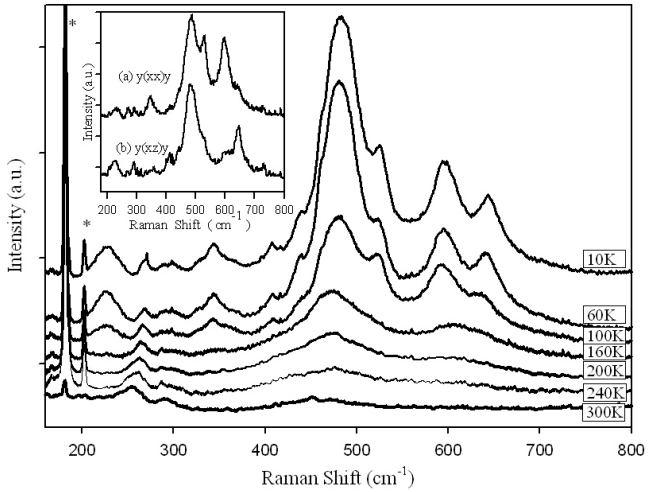

Figure 2. $Pr_{0.5}Ca_{0.5}MnO_3$ single-crystal A_g and B_{2g} Raman-active phonons as a function of temperature. * indicate plasma lines. Inset: (a) A_g phonons and (b) B_{2g} phonons at 10 K.

phonons were detected. The $Pr_{0.5}Ca_{0.5}MnO_3$ single-crystal DC magnetic susceptibility χ temperature dependence was measured using a home-made vibrating sample magnetometer to confirm the various magnetic phase evolutions. The DC susceptibility was determined via the measured magnetization in $H = 1.2$ kOe magnetic field ($\chi = M/H$). The corresponding magnetization curves were linear with H in the whole temperature range. Both heating and cooling regimes of the susceptibility measurements showed approximately similar results.

3. Results and discussion

The $Pr_{0.5}Ca_{0.5}MnO_3$ single-crystal DC susceptibility increases between 300 K and $T_{co} \sim 240$ K, indicating a tendency to a ferromagnetic phase (figure 1). At $T_{co} < T < T_N$, competition between ferromagnetism and antiferromagnetism, favored by charge ordering, reduces the susceptibility and quenches double exchange interaction [35]. Also, the antiferromagnetic phase transition at $T_N \sim 170$ K is marked by a bump in the susceptibility which is influenced at low temperatures by the Pr^{3+} ions.

In figure 2, $Pr_{0.5}Ca_{0.5}MnO_3$ single-crystal Raman spectra at temperatures between 300 and 10 K are presented. At 300 K, in the paramagnetic phase with ferromagnetic correlations, the $Pr_{0.5}Ca_{0.5}MnO_3$ space group is *Pnma* and three excitations ∼255, 290 and 450 cm^{-1}, induced by incoherent Jahn–Teller distortions, are observed. Below $T_{co} \sim 240$ K, the space group remains *Pnma* and charge ordering develops with new excitations around 470 and 590 cm^{-1}. Between T_{co} and T_N the unit cell parameters show sharp variations and below T_N, with the occurrence of CE-type antiferromagnetism and complete orbital ordering, the structure adopts a monoclinic symmetry ($P2_1/m$) [36]. We have also measured the Raman-active excitations under applied magnetic field parallel to the incident light up to 7 T. No significant changes in frequencies or linewidths were observed, confirming the robustness of the charge ordered phase.

Similarly to $Nd_{0.5}Ca_{0.5}MnO_3$ [25], a simplified *Pmma* structure characterized by charge and orbital ordering without octahedra tilts is used for the low temperature spectral analysis predicting nine external modes of stretching and bending types and twelve high frequency internal modes of translational and rotational types [23]. Sixteen Raman-active modes are observed and their frequencies are compared in table 1 to the corresponding excitations in $Nd_{0.5}Ca_{0.5}MnO_3$ [25].

Compared to $Nd_{0.5}Ca_{0.5}MnO_3$, $Pr_{0.5}Ca_{0.5}MnO_3$ Raman-active phonon frequencies are very close and vary by a few cm^{-1}. In both compounds typical manganite vibrations are observed at 343 cm^{-1} (out-of-phase octahedral tilting), 483 cm^{-1} (octahedral basal oxygen out-of-phase bending) and 595 cm^{-1} (octahedral basal oxygen-in-phase stretching). In contrast to $PrMnO_3$ for which the 492 cm^{-1} A_g and 608 cm^{-1} B_{2g} are softening noticeably as temperature is lowered below the A-type antiferromagnetic transition [37], the $Pr_{0.5}Ca_{0.5}MnO_3$ 483 and 595 cm^{-1} phonons do not soften and seem less affected by the CE-type antiferromagnetism. Also the 645 cm^{-1} density-of-states infrared-and Raman-active excitations in $PrMnO_3$, which play an important role in the multiphonon processes [38], are observed in $Pr_{0.5}Ca_{0.5}MnO_3$ at 643 cm^{-1}. Finally, the 307, 346 and 529 cm^{-1} A_g and 227, 410 and 443 cm^{-1} B_{2g} $Nd_{0.5}Ca_{0.5}MnO_3$ phonons, described in [25], find their corresponding modes in $Pr_{0.5}Ca_{0.5}MnO_3$ at 300, 343 and 524 cm^{-1} for the A_g and 227, 406 and 444 cm^{-1} for the B_{2g} modes, respectively. Due to the order–disorder transition from dynamical to static Jahn–Teller cooperative effect at low temperatures, the phonon intensities increase significantly. Also, as a result of orbital ordering and resultant changes in the Mn–O bond covalence, phonons with dominant oxygen motions in the xz plane harden significantly between 100 and 4.2 K (e.g. $\Delta\nu$ of the breathing stretching A_g

Table 1. Raman-active phonon frequencies at $T < T_N$ (in cm^{-1}) of $Pr_{0.5}Ca_{0.5}MnO_3$, PCMO/STO and PCMO/LAO as compared to $Nd_{0.5}Ca_{0.5}MnO_3$ published data. ($\Delta\nu$) corresponds to the frequency hardening between 100 and 10 K.

$Nd_{0.5}Ca_{0.5}MnO_3$ [25]	$Pr_{0.5}Ca_{0.5}MnO_3$	PCMO/STO	PCMO/LAO
A_g	A_g ($\Delta\nu$)	A_g ($\Delta\nu$)	A_g ($\Delta\nu$)
239	216(0)		
274	268(1)	268(1)	269(1)
295	287(0)	286(0)	286(0)
307	300(0)	295(0)	295(0)
331	328(0)	328(0)	328(0)
346	343(2)	342(2)	347(0)
367	359(0)	364(0)	364(0)
486	483(3)	486(5)	483(3)
529	524(4)	527(4)	531(5)
589	595(5)	599(3)	592(2)
634			
B_{2g}	B_{2g}	B_{2g}	B_{2g}
169		167(0)	167(0)
227	227(0)	230(0)	228(0)
410	406(0)	405(0)	411(0)
443	444(4)	438(2)	446(2)
464	459(0)	458(0)	460(0)
479	475(7)	473(5)	473(3)
490	498(0)	500(0)	501(0)
643	643(10)	646(0)	649(9)

595 cm^{-1}, the bending B_{2g} 475 cm^{-1} and the stretching B_{2g} 643 cm^{-1} modes in table 1).

The phonons of the high temperature phase persist below T_N. Even though such an observation is not a direct confirmation of the Zener polaron, it confirms that monoclinic and orthorhombic phases coexist in line with the observations of Wu *et al* [18] who detected also the formation of a Zener polaron. Also, the close similarities between $Nd_{0.5}Ca_{0.5}MnO_3$ and $Pr_{0.5}Ca_{0.5}MnO_3$ Raman-active phonon frequencies and intensities as well as their temperature evolution suggest that, if a Zener polaron is formed in $Pr_{0.5}Ca_{0.5}MnO_3$, it should be equally observed in $Nd_{0.5}Ca_{0.5}MnO_3$.

Fewer Raman-active broad phonons between 475 and 650 cm^{-1} have been observed by Dediu *et al* in $Pr_{0.65}Ca_{0.35}MnO_3$ [27]. It appears that in the $Pr_{0.5}Ca_{0.5}MnO_3$ single crystal where charge ordering is optimized and commensurate, the overall phonon spectral shapes and intensities as a function of temperature reflect a clear orbital ordering evolution and strong charge and spin–lattice couplings. Also, by using the 488 nm excitation laser line we observed no modification in the Raman spectra in contradiction to the drastic changes reported by Dediu *et al* [27] and assigned to photogenerated polarons.

The temperature dependence of the frequency and width of the 268 cm^{-1} $A_g(2)$ phonon is of particular interest (figures 3(a) and (b)). In this mode, only the in-plane oxygen atoms are involved with adjacent MnO_6 octahedra rotating in phase. Its low temperature frequency is hardening and its linewidth is increasing as temperature decreases: this behavior has been attributed to strong spin–phonon coupling written in terms of Schwinger boson operators by Gupta *et al* [28]. Dattagupta and Sood [29] have invoked the phonon–charge ordering interaction and its corresponding polaron-like

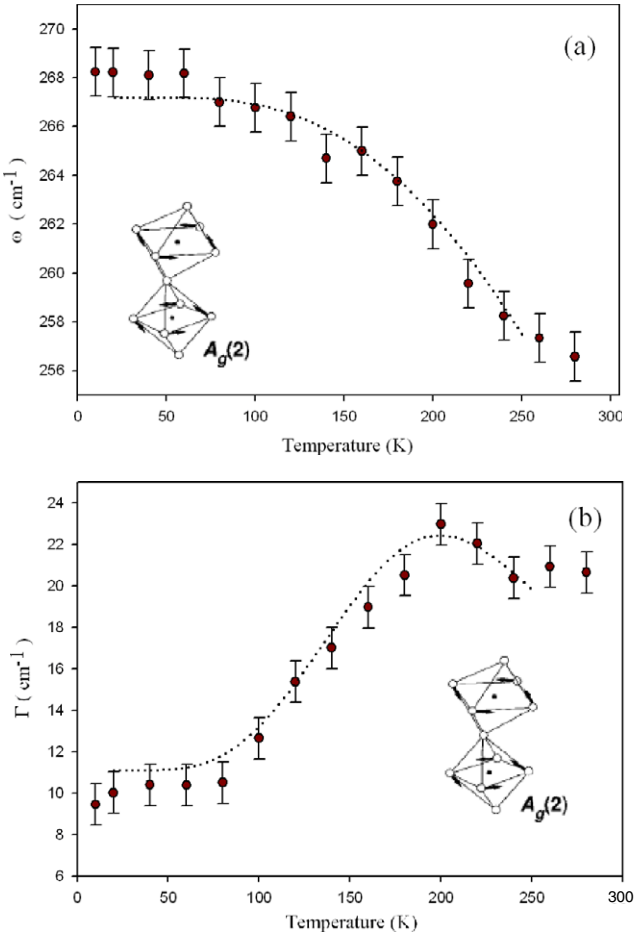

Figure 3. Temperature dependence of $Pr_{0.5}Ca_{0.5}MnO_3A_g(2)$ phonon frequency (a) and linewidth (b). Dotted lines correspond to the fit described in the text.

physics as a major player in the temperature dependence of the phonon frequency and linewidth. Nevertheless the resolution, as a function of temperature, of their studied $A_g(2)$ phonon in $Pr_{0.63}Ca_{0.37}MnO_3$ [28, 29] was poor and discriminating between the two models is not obvious.

With our improved detection of the 260 cm^{-1} A_g mode linewidth, the anomaly that characterizes the dominant interaction is clearly observed around $T_{co} \sim 240$ K rather than around $T_N \sim 170$ K. Hence the t_{2g} spin Hamiltonian of Gupta *et al* [28], which becomes effective near and below T_N, seems less adequate to describe the phonon linewidth temperature evolution around $T = 250$ K. Dattagupta and Sood [29] have adapted polaron-mediated tunneling rates for light interstitials in solids to the phonon–charge ordering interaction. The same coupling constant of the interaction which is derived from the low temperature frequency shift is used to analyze the temperature dependence of the linewidth. According to their calculations (see [29] for details), the phonon frequency shift $\Delta\omega$, the order parameter p and the phonon linewidth Γ are given by [29]:

$$\Delta\omega(T) = \frac{(gp)^2}{2\omega}, \qquad p = \tanh\left(\frac{pT_{co}}{T}\right),$$

$$\text{and} \qquad \Gamma(T) = \frac{g^2(1-p^2)}{(T+\gamma T^7)} \tag{1}$$

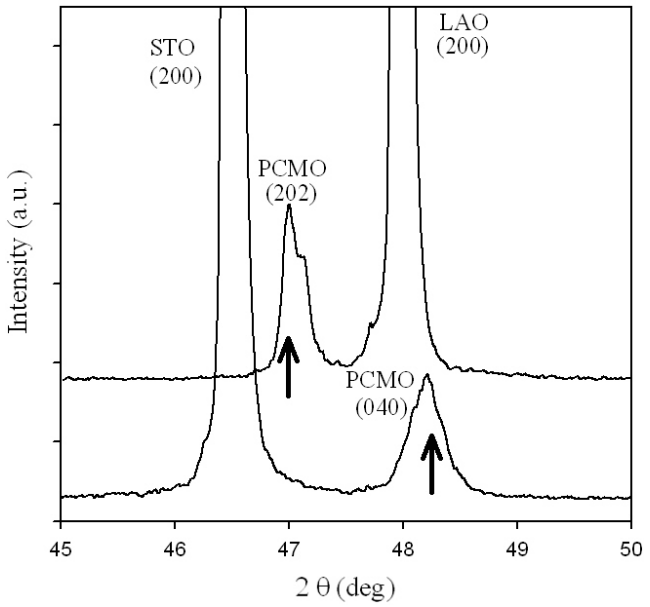

Figure 4. X-ray diffraction pattern at room temperature of 2000 Å $Pr_{0.5}Ca_{0.5}MnO_3$ (PCMO) thin films on $SrTiO_3$ (STO) and $LaAlO_3$ (LAO) around 47°.

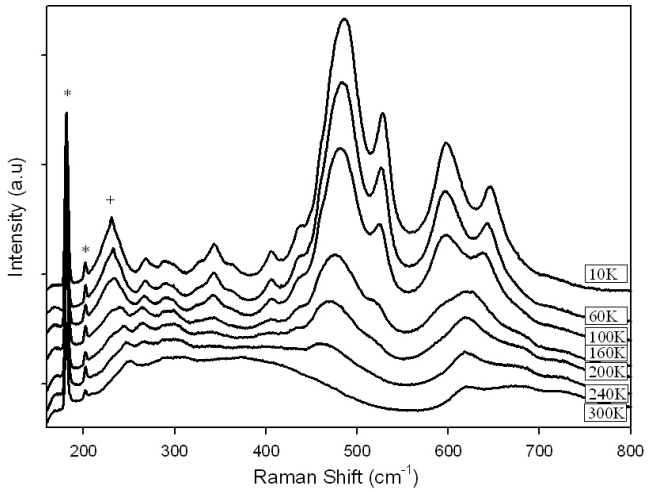

Figure 5. 2000 Å PCMO/STO thin film Raman-active phonons as a function of temperature. * indicates plasma lines and + substrate phonons.

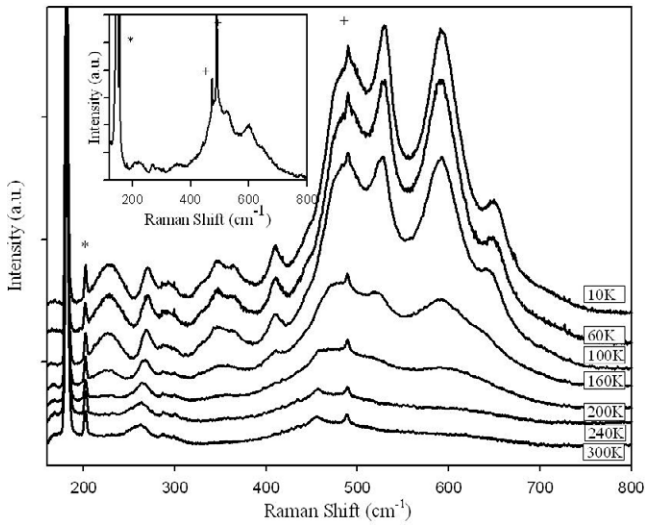

Figure 6. 2000 Å PCMO/LAO thin film Raman-active phonons as a function of temperature. * indicates plasma lines and + substrate phonons. Inset: 200 Å PCMO/LAO thin film phonons at $T = 10$ K.

with ω being the phonon frequency, g the phonon–charge ordering coupling constant and p the temperature-dependent charge order parameter. Both one-phonon and two-phonon processes are considered in the linewidth term with relaxation terms proportional to T and T^7, respectively, and a fitting parameter γ estimated to be 10^{-14}. $\Delta\omega$ and Γ as a function of temperature are well fitted with $g = 80.6\ \mathrm{cm}^{-1}$ (figures 3(a) and (b)) in comparison to $g = 36.7\ \mathrm{cm}^{-1}$ as calculated in $Pr_{0.63}Ca_{0.37}MnO_3$ [29]. It thus appears that in $Pr_{0.5}Ca_{0.5}MnO_3$, the phonon–charge ordering interaction is dominant and the polaron-like model is well adapted to describe it above T_N.

A preliminary x-ray study of our 2000 Å PCMO thin films, deposited on (LAO) and (STO) [100] substrates, indicates that the films are oriented along the [101] ($a \sim c = 5.44$ Å) and [010] ($b = 7.54$ Å) directions, respectively (figure 4). The bulk $Pr_{0.5}Ca_{0.5}MnO_3$ lattice parameters being $a = 5.395$ Å, $b = 7.612$ Å and $c = 5.403$ Å, our x-ray data show that our PCMO films remain under compressive and tensile in-plane strains for LAO and STO, respectively, similar to $Nd_{0.5}Ca_{0.5}MnO_3$ films [30].

In figures 5 and 6, Raman spectra of PCMO/STO and PCMO/LAO thin films at different temperatures are shown and look very similar to the spectra obtained with the $Nd_{0.5}Ca_{0.5}MnO_3$ thin films [30]. The Raman excitations from the STO and LAO substrates are visible in the spectra and dominate in the case of PCMO/STO at room temperature. In contrast to previous Raman studies of PCMO/STO and PCMO/LAO thin films deposited at 725 °C, where orbital ordering is not detected [31, 32], we observe the CE-type antiferromagnetic and the orbital ordering transitions (table 1) with strong characteristic excitations (e.g. for PCMO/STO: 486, 527, 599 and 646 cm^{-1} and for PCMO/LAO: 483, 531, 592 and 649 cm^{-1}) emerging at low temperatures from the two substrate backgrounds. This is a clear indication that the stoichiometry, with the absence of local modes and minimum strains, is improved in our films by using higher substrate temperatures during the deposition ($T_{\mathrm{substrate}} = 820\,^{\circ}\mathrm{C}$). CE-type transition Raman excitations of the 200 Å thin film PCMO/LAO at $T = 5$ K (figure 6 inset) are also observed. Even though broadened by interface strains, they indicate the ability of the charge and orbital ordering phase transitions to develop even in reduced thicknesses for PCMO/LAO thin films.

Finally, fitting the $A_g(2)$ phonon $\Delta\omega(T)$ and $\Gamma(T)$ with relations (1) confirms the close similarities between the PCMO/LAO thin film and the $Pr_{0.5}Ca_{0.5}MnO_3$ single crystal. The data in both cases are well reproduced with $g = 80.6\ \mathrm{cm}^{-1}$ and $T_{co} = 250$ K. However, for PCMO/STO thin films, a best fit is realized with $g = 45\ \mathrm{cm}^{-1}$ and $T_{co} = 220$ K, reflecting the influence of the tensile stress that results in a weaker

phonon–charge order coupling in addition to an important decrease of charge order melting magnetic field [20].

The overall phonon frequencies and their temperature dependence in $Pr_{0.5}Ca_{0.5}MnO_3$ and $Nd_{0.5}Ca_{0.5}MnO_3$ single crystals and thin films are very alike. These phonon signatures confirm the similarities of their T_{co}, T_N and magnetic field dependence of resistivity and magnetization at fixed temperatures [39]. Thus, we expect $Nd_{0.5}Ca_{0.5}MnO_3$ to be a good candidate for an experimental confirmation of Zener-polaron-type charge and orbital orders as reported recently in $Pr_{0.5}Ca_{0.5}MnO_3$.

4. Conclusion

The impact of charge ordering and the transition to the CE-type antiferromagnetic phase in $Pr_{0.5}Ca_{0.5}MnO_3$ single crystal and thin films have been studied by micro-Raman scattering and compared with previous results. Similarly to $Nd_{0.5}Ca_{0.5}MnO_3$, the persistence at low temperatures of phonons from the high temperature ferromagnetic phase and of the A-type antiferromagnetic phase corroborates a phase separation scenario. Also, the MnO_6 octahedra phonon symmetries and profiles in the CE-type phase indicate coherent cooperative Jahn–Teller distortions. The well-resolved temperature dependence of the frequency and linewidth of the 260 $cm^{-1}A_g$ phonon suggests a strong coupling with the charge ordering. The similarities between both charge ordered manganites should extend to the observation of the Zener polaron not yet confirmed in $Nd_{0.5}Ca_{0.5}MnO_3$.

In contrast to previous Raman reports on $Pr_{0.5}Ca_{0.5}MnO_3$ and $La_{0.5}Ca_{0.5}MnO_3$ thin films, we observe in our PCMO/LAO and PCMO/STO thin films additional phonon excitations that are associated with the CE-type antiferromagnetic phase transition. We conjecture that the higher substrate temperature favors defect-free thin films with properties similar to the single crystals.

Acknowledgments

We acknowledge the technical support of S Pelletier and M Castonguay, and the financial support from the National Science and Engineering Research Council of Canada, the Fonds Québécois de la Recherche sur la Nature et les Technologies, the Canadian Institute for Advanced Research, the Canada Foundation for Innovation and the Program of Quantum Phenomena in Condensed Matter of the Russian Academy of Sciences and Russian Foundation for Basic Researches.

References

[1] Zener C 1951 *Phys. Rev.* **82** 403
[2] Ramirez A P 1997 *J. Phys.: Condens. Matter* **9** 8171
[3] Imada M, Fujimori A and Tokura Y 1998 *Rev. Mod. Phys.* **70** 1039
[4] Dagotto E 2003 *Nanoscale Phase Separation and Colossal Magnetoresistance* (*Springer Series in Solid-State Sciences*) (New York: Springer)
[5] Jim S, Tiefel T H, McCormack M, Fastnacht R, Ramesh R and Chen L H 1994 *Science* **264** 413
[6] Khomskii D I and Sawatzky G A 1997 *Solid State Commun.* **102** 87
[7] Woodward P M, Vogt T, Cox D E, Arulraj A, Rao C N R, Karen P and Cheetham A K 1998 *Chem. Mater.* **10** 3652
[8] Coey J M D, Viret M and von Molnar S 1999 *Adv. Phys.* **48** 167
[9] Uehara M, Mori S, Chen C H and Cheong S W 1999 *Nature* **399** 560
[10] Rao C N R, Arulraj A, Cheetham A K and Raveau B 2000 *J. Phys.: Condens. Matter* **12** R83
[11] Goodenough J B 1955 *Phys. Rev.* **100** 564
[12] Radaelli P G, Cox D E, Marezio M and Cheong S W 1997 *Phys. Rev.* B **55** 3015
[13] Tomioka Y, Asamitsu A, Kuwahara H, Moritomo Y and Tokura Y 1996 *Phys. Rev.* B **53** R1689
[14] Grenier S, Hill J P, Gibbs D, Thomas K J, Zimmermann M v, Nelson C S, Kiryukhin V, Tokura Y, Tomioka Y, Casa D, Cog T and Venkataraman C 2004 *Phys. Rev.* B **69** 134419
[15] Trokiner A, Yakubovskii A, Verkhovskii S, Gerashenko A and Khomskii D 2006 *Phys. Rev.* B **74** 092403
[16] Goff R J and Attfield J P 2004 *Phys. Rev.* B **70** 140404(R)
[17] Daoud-Aladine A, Rodriguez-Carvajal J, Pinsard-Gaudart L, Fernandez-Diaz M T and Revcolevschi A 2002 *Phys. Rev. Lett.* **89** 097205
[18] Wu L, Klie R F, Zhu Y and Jooss Ch 2007 *Phys. Rev.* B **76** 174210
[19] Haghiri-Gosnet A M, Hervieu M, Simon Ch, Mercy B and Raveau B 2000 *J. Appl. Phys.* **88** 3545
[20] Prellier W, Haghiri-Gosnet A M, Mercey B, Lecoeur Ph, Hervieu M, Simon Ch and Raveau B 2000 *Appl. Phys. Lett.* **77** 1023
[21] Iliev M N and Abrashev M V 2001 *J. Raman Spectrosc.* **32** 805
[22] Weber W H and Merlin R 2000 *Raman Scattering in Materials Science* (*Springer Seriesin Materials Science*) (Berlin: Springer)
[23] Abrashev M V, Bäckström J, Börjesson L, Pissas M, Kolev N and Iliev M N 2001 *Phys. Rev.* B **64** 144429
[24] Asselin A, Jandl S, Fournier P, Mukhin A A, Ivanov V Yu and Balbashov A M 2005 *J. Phys.: Condens. Matter* **17** 5247
[25] Jandl S, Mukhin A A, Ivanov V Yu and Balbashov A M 2006 *J. Phys.: Condens. Matter* **18** 1667
[26] Dagotto E, Burgy J and Moreo A 2003 *Solid State Commun.* **126** 9
[27] Dediu V, Ferdeghini C, Matacotta F C, Nozar P and Ruani G 2000 *Phys. Rev. Lett.* **84** 4489
[28] Gupta R, Venketeswara Pai G, Sood A K, Ramakrishnan T V and Rao C N R 2002 *Europhys. Lett.* **58** 778
[29] Dattagupta S and Sood A K 2002 *Phys. Rev.* B **65** 064405
[30] Charpentier S, Gill-Comeau M, Jandl S and Fournier P 2006 *J. Phys.: Condens. Matter* **18** 7193
[31] Xiong Y M, Chen T, Wang G Y, Chen X H, Chen X and Chen C L 2004 *Phys. Rev.* B **70** 094407
[32] Tatsi E, Papadopoulo E L, Lampakis D, Liaropakis E, Prellier W and Mercey B 2003 *Phys. Rev.* B **68** 024432
[33] Antonakos A, Palles D, Liarokapis E, Filippi M and Prellier W 2008 *J. Appl. Phys.* **104** 063508
[34] Balbashov A M, Karabashev S G, Mukovskiy Ya M and Zverkov S A 1996 *J. Cryst. Growth* **167** 365
[35] Pollert E, Krupicka S and Kuzmicova E 1982 *J. Phys. Chem. Solids* **43** 1137
[36] Jirak Z, Damay F, Hervieu M, Martin C, Raveau B, André G and Bourée F 2000 *Phys. Rev.* B **61** 1181
[37] Laverdière J, Jandl S, Mukhin A A, Ivanov V Yu, Ivanov V G and Iliev M N 2006 *Phys. Rev.* B **73** 214301
[38] Laverdière J, Jandl S, Mukhin A A and Ivanov V Yu 2006 *Eur. Phys. J.* B **54** 67
[39] Tokura Y and Tomioka Y 1999 *J. Magn. Magn. Mater.* **200** 1